Anal Bioanal Chem (2011) 401:809–816
DOI 10.1007/s00216-011-4986-3

ORIGINAL PAPER

Imaging the cellular uptake of tiopronin-modified gold nanoparticles

Xiaoqing Cai · Hsiang-Hsin Chen · Cheng-Liang Wang · Shin-Tai Chen · Sheng-Feng Lai · Chia-Chi Chien · Yi-Yun Chen · Ivan M. Kempson · Yeukuang Hwu · C. S. Yang · G. Margaritondo

Received: 11 January 2011 / Revised: 1 April 2011 / Accepted: 5 April 2011 / Published online: 3 May 2011

Abstract Well-dispersed gold nanoparticles (NP) coated with tiopronin were synthesized by X-ray irradiation without reducing agents. High-resolution transmission electron microscopy shows that the average core diameters of the NPs can be systematically controlled by adjusting the tiopronin to Au mole ratio in the reaction. Three methods were used to study the NP uptake by cells: quantitative measurements by inductively coupled plasma mass spectrometry, direct imaging with high lateral resolution transmission electron microscopy and transmission X-ray microscopy. The results confirmed that the NP internalization mostly occurred via endocytosis and concerned the cytoplasm. The particles, in spite of their small sizes, were not found to arrive inside the cell nuclei. The synthesis without reducing agents and solvents increased the biocompatibility as required for potential applications in analysis and biomedicine in general.

Keywords Gold nanoparticles · X-ray synthesis · Cellular uptake · Transmission X-ray microscopy

Published in the special issue *Imaging Techniques with Synchrotron Radiation* with Guest Editor Cyril Petibois.

Electronic supplementary material The online version of this article (doi:10.1007/s00216-011-4986-3) contains supplementary material, which is available to authorized users.

X. Cai · H.-H. Chen · C.-L. Wang · S.-T. Chen · S.-F. Lai · C.-C. Chien · Y.-Y. Chen · I. M. Kempson · Y. Hwu (✉)
Institute of Physics, Academia Sinica,
Nankang,
Taipei 11529, Taiwan
e-mail: phhwu@sinica.edu.tw

C.-C. Chien · Y. Hwu
Department of Engineering and System Science,
National Tsing Hua University,
Hsinchu 300, Taiwan

Y. Hwu
Institute of Optoelectronic Sciences,
National Taiwan Ocean University,
Keelung 202, Taiwan

C. S. Yang
Center for Nanomedicine, National Health Research Institutes,
Miaoli, Taiwan

G. Margaritondo
Ecole Polytechnique Fédérale de Lausanne (EPFL),
1015, Lausanne, Switzerland

Introduction

Different types of gold nanostructures were developed and extensively analyzed in recent years [1–3]. Among them, thiol-stabilized gold nanoparticles are particularly attractive for their potential applications in nanoelectronics, catalysis, optics, chemical and biological sensing, and biomedicine [4–15]. The stabilizing surfactants prevent aggregation, as required to control the chemical reactions and subsequently the size and its uniformity. Furthermore, most nanoparticles must be functionalized for specific applications after the surface is passivated. Free bonding sites on the surfactant that can facilitate further surface conjugation are therefore desirable to simplify the reactions. The strong bonding of thiol groups to Au makes it particularly suitable for this purpose.

The synthesis of dodecanethiol-stabilized nanoparticles was previously developed using a biphasic method [4] taking advantage of phase-transfer compounds to transfer ionic reagents to an organic phase in which particle nucleation, growth, and passivation can occur. In such a synthesis, the stabilizing thiol ligands must be compatible

with all the reagents, such as $NaBH_4$ and the phase-transfer catalysts, and are therefore vulnerable to contamination by residual reagents. Water soluble clusters with an average diameter of 1.8 nm synthesized in a single aqueous phase active process were recently reported [8]. Phase-transfer catalysts and other organic solvents, except methanol, were not required; and the dried nanoparticle powders were stable and re-dispersible in water. The free terminal carboxyl group could be exploited to obtain further functionality. Many clusters of this type were synthesized with atomic-level precision, and their structural properties were determined by X-ray crystallography [16–18].

In addition to the chemical reduction using $NaBH_4$, other methods such as γ-ray [19] and X-ray [20, 21] irradiation have been demonstrated to be capable of replacing reduction agents for synthesizing well-dispersed AuNPs. Reduction using highly penetrating irradiation can normally produce a uniform reaction which is a common concern in processes involving more than one chemical. The X-rays generated by synchrotron sources have extremely high intensity and therefore offer additional advantages in guaranteeing very fast and complete reactions with respect to other irradiation sources used in the synthesis of metallic nanoparticles in solution. Many reactions that were otherwise impossible or difficult can be implemented with this new method [22–25]. This approach also offers room temperature processing, high reproducibility, fast reaction rates, complete reaction, and the elimination of complicated procedures to remove residual chemicals. High yield, high biocompatibility, and a simplified chemical process are positive factors that could justify the access cost to a synchrotron facility.

For biomedical application, a key issue is the stability in physiological conditions and the potential toxicity to the cell. Tiopronin (*N*-(2-mercaptoproionyl)glycine) is a pharmaceutical drug used for the treatment of cystinuria and rheumatoid arthritis, and its basic biocompatibility is therefore quite well established. Possessing a thiol group, it is also often used as a stabilizing agent to prevent aggregation and therefore control particle size [8]. The free carboxyl group of the tiopronin is available for covalent coupling to various linkers for further modification and functionalization.

The intracellular uptake and its spatial distribution are also of crucial importance for biomedical applications [26–28]. The cellular distribution of nanoparticles is commonly studied by optical microscopy and transmission electron microscopy (TEM) [27–31]. The latter offers sufficient resolution to image the nanoparticles and to provide information on their 2D distribution on thin specimens (<1 μm). However, the corresponding preparation processes involving dehydration, embedding, and other steps are normally time-consuming and can lead to artifacts. Transmission X-ray microscopy (TXM) was demonstrated to be an effective imaging method to study nanoparticle distributions at sub-cellular level providing sufficient lateral resolution to image the uptaken particles [32, 33]. The advantage of using highly penetrating X-rays to examine thick samples and the corresponding tomographic reconstruction to reveal 3D localization is particularly useful for the analysis of uptaken nanoparticles in single cells and cell clusters [34, 35].

The size and properties of the tiopronin-coated AuNPs was characterized with UV–Vis spectra and FTIR spectroscopy, in particular, to demonstrate that the characteristics of the final products can be controlled by irradiating different tiopronin/$AuCl_4^-$ mixtures. The overall, averaged cellular uptake was quantitatively analyzed using inductively coupled plasma mass spectrometry (ICP-MS). High-resolution TEM (HRTEM) corroborated the results on the internalization and morphology of the aggregates.

Experimental

Materials

N-(2-Mercaptopropionyl)glycine (tiopronin, 99%) and hydrogen tetrachloroaurate trihydrate ($(HAuCl_4 \cdot 3H_2O)$) were acquired from Aldrich Sigma (St. Louis, MO)). Dulbecco's modified Eagle medium (DMEM)-F-12 medium and fetal bovine serum were from Invitrogen (Paisley, UK). Water was purified by passing house-distilled water through a Millipore NANOpure system (>18 MΩ). EMT-6 cells were obtained from American Type Culture Collection. All chemicals were reagent grade and used as received.

X-ray synthesis of tiopronin-coated AuNPs

The one-pot synthesis used intense X-ray irradiation produced by the BL01A beamline of the National Synchrotron Radiation Research Center (NSRRC, Hsinchu, Taiwan) with an electron storage ring current of 360 mA. A detailed description of the beamline was reported elsewhere [36]. The photon energy distribution was centered at ~12 keV, and the dose rate was 5.1±0.9 kGy s^{-1} as measured by a Fricke dosimeter with an estimated *G* value of 13.

The reaction took place in aqueous solution without any reductant or organic solvent. In a typical process, 0.078 g of tetrachloroauric acid (0.20 mmol) and 0.031 g of *N*-(2-mercaptopropionyl)glycine (0.20 mmol) were dissolved in 10 ml of deionized water in a 15-ml polypropylene conical tube (Falcon®, Becton Dickinson, NJ), giving a ruby red solution. The solution was irradiated for 5 min and its color changed to black. The solution was purified by dialysis, using 8-in. segments of cellulose ester dialysis membrane (Millipore, MWCO=10 K), placed in 5-l beakers of deionized water, and stirred slowly, recharging with fresh

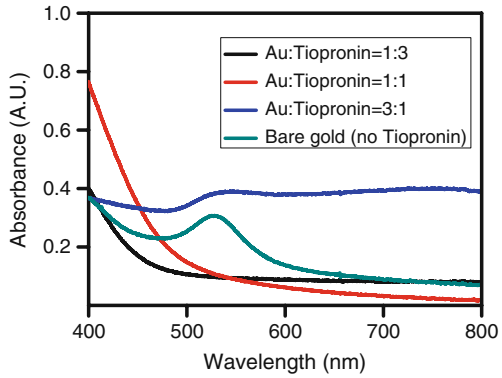

Fig. 1 UV–visible spectra of tiopronin-coated AuNPs synthesized by synchrotron X-ray irradiation

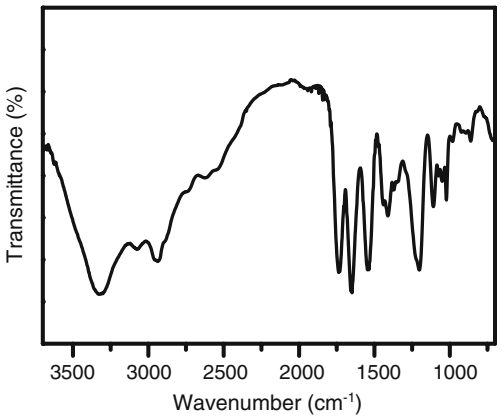

Fig. 3 Transmission FTIR spectra of tiopronin-coated AuNPs synthesized with a molar ratio of 1:1

water every 10 h over 72 h. The dark blue tiopronin–AuNP solutions were collected from the dialysis membrane, and the solvent was removed under vacuum at ≤40 °C.

Characterization of tiopronin-coated AuNPs

UV–Vis absorption spectra were recorded with a Shimadzu UV-160 spectrometer (200–800 nm, 1 nm resolution) with a 1-cm quartz cuvette. TEM analysis was performed with a JEOL JEM 2010F field emission gun transmission electron microscope (FEG-TEM) operating at 200 kV. The samples for TEM measurements were prepared by placing droplets of nanoparticle-containing solution on carbon-coated Cu grids and were allowed to dry in room atmosphere. The infrared spectra of dried samples on a silicon wafer were recorded in the spectral range of 4,000–1,000 cm^{-1} using a FTIR spectrometer (Spectrum One, Perkin-Elmer).

Cytotoxicity of tiopronin-coated AuNPs

EMT-6 cells were separately cultured in DMEM-F-12 medium supplemented with 1% penicillin–streptomycin and 10% fetal bovine serum. For the cytotoxicity assays, cells in the multiplate were treated for 24 h with different concentrations of 0.2, 0.5, 1, and 2 mg/ml of tiopronin–AuNP. Culture media without gold nanoparticles served as control specimens. After the end of the incubation time, the cells were harvested and stained with trypan blue reagent to direct count the live cell numbers. All experiments were repeated three times, and the data are presented as the mean±S.E.

ICP-MS analysis

EMT-6 cells were exposed to 200 μg/ml tiopronin–AuNP in cell culture medium for 0, 1, 2, 4, 6, 12, and 24 h to measure the nanoparticle uptake by the cells. The cells were exposed to different concentrations of nanoparticles (10, 20, 50, 100, 200, and 500 μg/ml) for 24 h. After different incubation times with different concentrations of nanoparticles, the culture medium was removed and washed with phosphate-buffered saline (PBS) three times, and the cells were digested with trypsin solution for 10 min. Sonication followed for 2 h in a hot water bath to completely disrupt the cell membranes. Finally, the gold nanoparticles were dissolved by successively adding 0.4 ml aqua regia (the volume ratio of 37% HCl and 70% HNO_3 was 3:1). The solution was diluted with deionized water

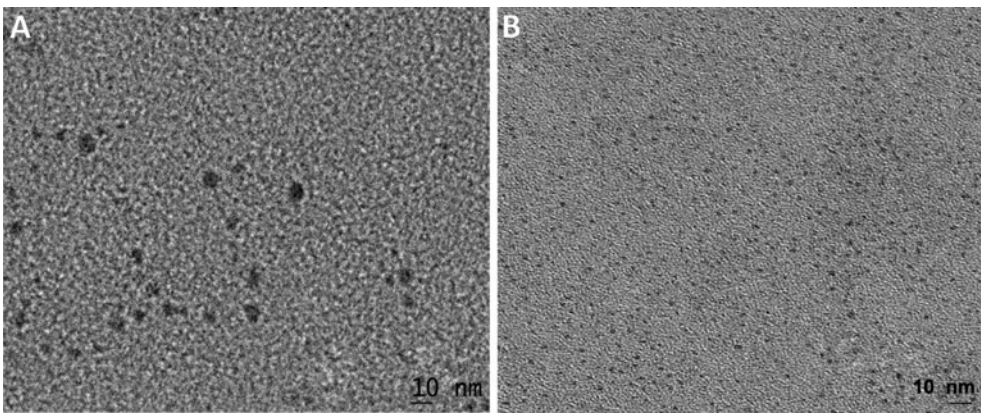

Fig. 2 TEM images with nanoparticles synthesized with Au:tiopronin molar ratios of (**A**) 1:1 and (**B**) 1:3

Table 1 Selected FTIR band assignments and positions for tiopronin and tiopronin–AuNPs

Tiopronin	Tiopronin–gold	Assignment
1,557 (s)	1,536 (s)	Amide II
1,622 (s)	1,646 (s)	Amide I
1,754 (s)	1,733 (s)	C=O stretch
2,565 (m)		S–H stretch
3,091 (s)	2,937 (br)	Amide B
3,316 (s)	3,330 (br)	Amide A

Only bands of significant intensity and relevance to confirm the presence or absence of hydrogen bonding are considered here. The peak positions are in cm^{-1}, and the peak intensity and the width are labeled as strong (s), medium (m), and broad (br)

until the HCl concentration reached 2% (*v*). The concentration of gold was determined by ICP-MS (ICP-MS 7500 CS, Agilent Technologies, USA).

Transmission electron microscopy

EMT-6 cells were seeded in six-well plates (Corning, Lowell, USA) at a density of 3.0×10^6 cells per well in 4 ml of culture medium. All cells were exposed to tiopronin-coated AuNPs after 60% confluence. The particle concentration was 200 μg/ml. After incubation for 12 h, the cells were fixed with 2.5% glutaraldehyde in 0.1 M PBS and washed. After post-fixation in 1% OsO_4 in PBS for 1 h, the cells were dehydrated by a series of ethanol rinsing processes, treated with propylene oxide, and then embedded in Epon. Thick sections of ~60–70 nm were cut on a LKB-Ultrotome V and transferred to Formvar-coated copper grids. The sections were stained with uranyl acetate and Reynolds lead citrate and examined with a JEOL JEM 2010F FEG-TEM operating at 200 kV.

X-ray microscopy analysis

Transmission X-ray microscopy was performed at the 32-ID beamline of the Advanced Photon Source, Argonne National Laboratory, USA, and the 01B beamline of NSRRC [30]. The suspended cells were grown on the Kapton support films overnight to obtain complete cell attachment in the films. After adding 200 μg/ml tiopronin–AuNPs for 12 h, the cells in the films were rinsed in 0.1 M PBS. The cells were fixed with 2.5% glutaraldehyde in 0.1 M PBS and washed. They were then dehydrated using a series of ethanol rinsing steps (30%, 50%, 70%, 90%, and 100%, for 30 min each). To obtain 3D tomographically reconstructed pictures, raw images were collected at different angles with 1° increments. The 3D reconstruction was processed with Xradia software and displayed with Amira. For quantitative analysis, the images were segmented manually and analyzed with the Image-Pro software.

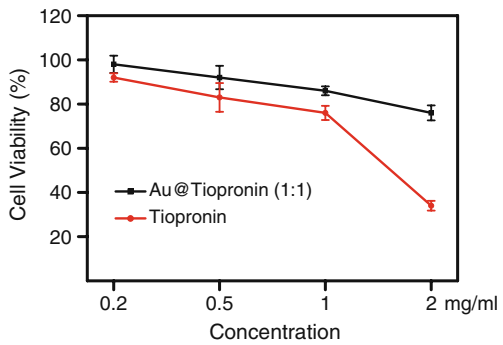

Fig. 4 Cytotoxicity profiles of tiopronin-coated AuNPs and tiopronin. The results are shown as mean±S.E.

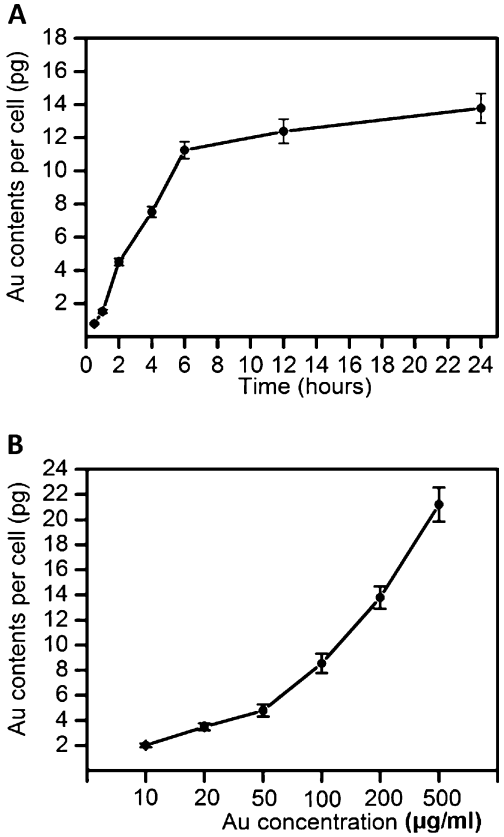

Fig. 5 (**A**) ICP-MS analysis of EMT-6 cells following different incubation times (0, 1, 2, 4, 6, 12, and 24 h) with medium containing 200 μg/ml tiopronin–AuNP. (**B**) ICP-MS analysis of EMT-6 cells exposed to different concentrations of tiopronin–AuNP (10, 20, 50, 100, 200, and 500 μg/ml)

Results and discussion

Synthesis and characterization of tiopronin-coated AuNP

Figure 1 shows the UV–Vis spectrum of gold nanoparticles synthesized and surface conjugated with tiopronin. The

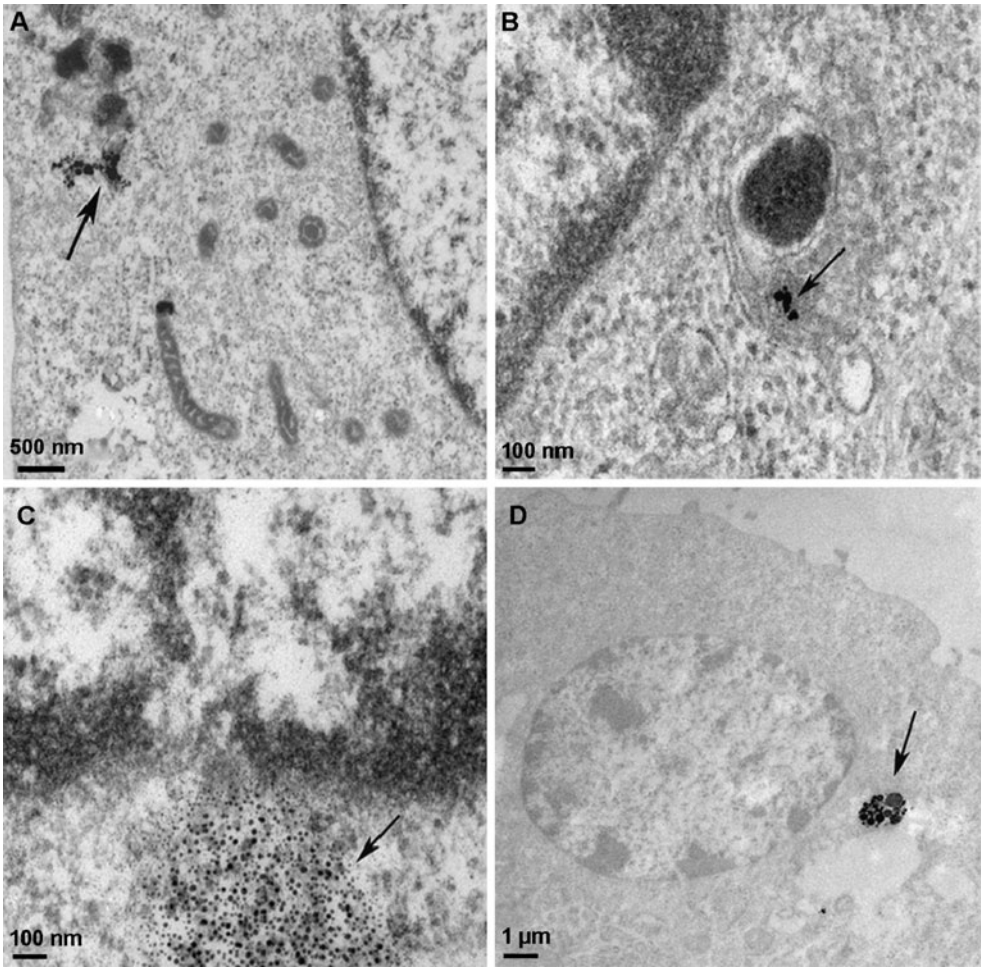

Fig. 6 TEM images of tiopronin-coated AuNPs internalization in EMT-6 cells. The *arrows* denote the NPs and the corresponding aggregates

spectra of this type depend on the core (metallic) size of the nanoparticles [8]. The AuNP core size was controlled by adjusting the molar ratio of tiopronin and Au. When the molar ratio of tiopronin to Au^{3+} ranged from 1:1 to 3:1, there was no detectable surface plasmon band, indicating that the average of the particle size was smaller than 2 nm [37]. When the molar ratio decreased to 1:3, the surface plasmon band could be detected at $\lambda_{max} \approx 522$ nm due to the larger core size of the nanoparticles. The size was confirmed by HRTEM. For example, for a ratio of 1:1 (Fig. 2), the size was found to be ~2 nm; and for a ratio of 3:1, the size was ~1 nm.

FTIR spectra of the tiopronin–AuNP are shown in Fig. 3. The peak positions and band assignments are summarized in Table 1. The amide A bands (3,300 cm^{-1}) correspond to N–H stretching vibrations, while the amide B band (2,937 cm^{-1}) is a Fermi resonance-enhanced overtone of the amide II band. The stretching band of the amide carbonyl (amide 1) normally appears at 1,630–1,680 cm^{-1}. The amide II band (1,500–1,600 cm^{-1}) arises from N–H and C–N torsional motions. The presence and the location of the various amide bands are of particular interest in determining the nature of hydrogen-bonding interactions within the tiopronin–gold ligand environment. These results are also consistent to those for chemically synthesized tiopronin-coated AuNPs [8].

The absence of a –SH stretch at 2,565 cm^{-1} in the infrared spectra confirms that the –SH proton is not present in the reactions indicating the formation of the tiopronin monolayer-protected Au core.

Effects on cell viability

The cell viability of the different concentrations of tiopronin–AuNP was evaluated by direct counting cellular numbers assays [38] of EMT-6 cells (a murine breast carcinoma cell line). The tumor animal model induced by this cell line is well established [39]. We previously investigated the uptake by these cells of different types of nanoparticles [38, 40, 41]. Furthermore, synchrotron X-ray imaging revealed early-stage tumors induced by EMT-6 cell inoculation and the local accumulation of nanoparticles [42]. We also used the standard MTT functional assay to evaluate the cellular toxicity but found that the dark color

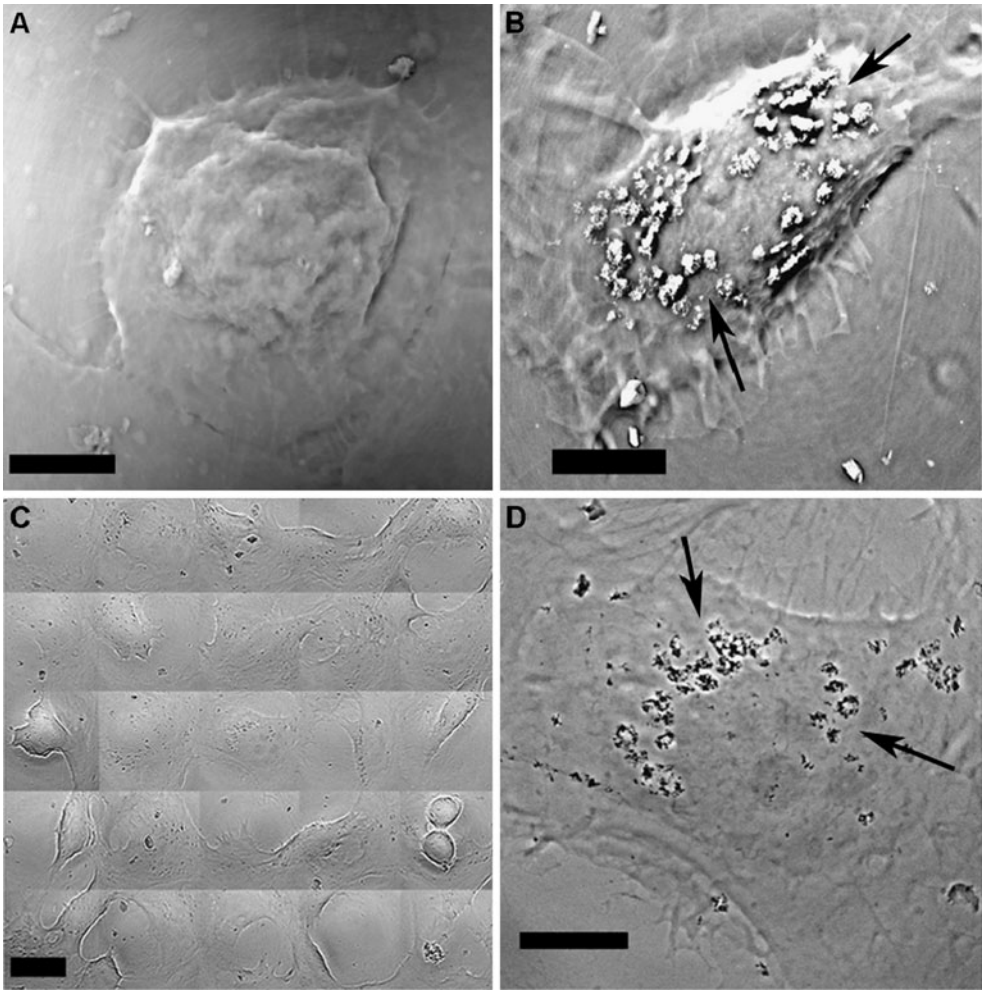

Fig. 7 Transmission X-ray microscope images. (**A**) A normal EMT-6 cell (control image). (**B**) Phase contrast TXM image of tiopronin-coated AuNPs in an EMT-6 cell. (**C**) Patchwork TXM images of EMT-6 cells incubated with our NPs. (**D**) Absorption contrast TXM image of tiopronin–AuNPs in the EMT-6 cells. *Scale bar*=5 μm

related to the nanoparticles interferes with the measurements and affects their reliability [43]: we thus adopted direct counting.

EMT-6 cells were cultured in media containing different concentrations of the tiopronin-coated AuNPs. As the concentration increased (from 0.2 to 2 mg/ml) in the culture medium, cell viability was not significantly altered (only a 24% decrease in cell viability at 2 mg/ml at 24 h). However, significant cytotoxicity was observed after 48 h at high concentration. When compared to the control group, cells cultured in medium containing 2 mg/ml tiopronin for 48 h exhibited only a 66% decrease in viability (Fig. 4).

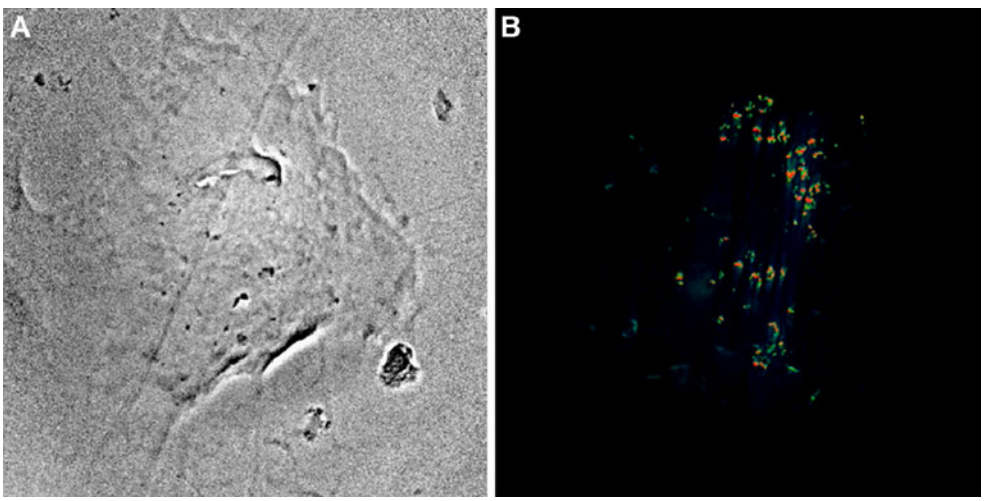

Fig. 8 Pictures produced by 3D tomography reconstruction confirming the internalization of tiopronin-coated AuNPs by EMT-6 cells. (**A**) Tomographic image of EMT-6 cells co-cultured with our NPs. (**B**) 3D reconstructed tomography by TXM. The tiopronin-coated AuNPs in the cells are also shown in the 3D movie (Supplementary Material)

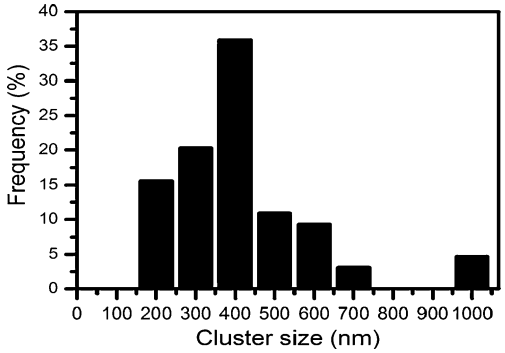

Fig. 9 Quantitative analysis of tiopronin-coated AuNPs uptake in EMT-6 cells

These results essentially demonstrated that tiopronin-coated AuNPs were less toxic than tiopronin to the EMT-6 cells even for high concentrations and long incubation times. The toxicity of gold–tiopronin (1:1) measured here (Fig. 4) is also less than the previous reports [44, 45]. This is reasonable considering that less chemicals, reducing agents, and other stabilizing agents are used in our synthesis process [22–24].

Uptake and intracellular distribution of tiopronin–AuNPs in EMT-6 cells

Nanoparticle internalization within cells is a potentially important factor for practical applications [46]. The cellular uptake was investigated by ICP-MS. As shown in Fig. 5A, for the first five incubation times (up to 6 h), the Au contents gradually increased, but then saturated for longer incubations. The cellular uptake also depended on the NP concentration: the Au uptake increased when the concentration increased from 10 to 500 μg/ml.

It is generally believed that nanoparticles internalized in cells remain in the endosome due to the endocytosis process [47]. As shown in Fig. 6A, tiopronin–AuNP aggregated in the cytoplasm around the cellular membrane. Caveolae are the major non-clathrin-dependent route from the cell surface to endosomes [48]. In our TEM study, tiopronin-coated Au aggregates were often found in the caveolae-like structure. For example, in Fig. 6B, NPs were found in the endosomes (Fig. 6B) and were surrounded by a membrane suggesting that they were taken into the endosome from the cytosol by caveolae. Interestingly, many tiopronin-coated AuNPs do not aggregate in the endosome, but are found freely dispersed in the cytosol (Fig. 6C), although the endosomal uptake mechanism remains dominant. The TEM image of Fig. 6D also shows that tiopronin-coated AuNPs are distributed in the cytoplasm of EMT-6 cells, but we did not observe NPs in the cell nucleus.

The above results were corroborated by TXM analysis. As shown in Fig. 7A, the cell membrane and the nanoparticles can be clearly imaged. The NP distribution is mainly in the cytoplasm and involves aggregation (Fig. 7B and D).

As shown in the 3D reconstructed tomography pictures of Fig. 8A and B, we clearly see that most of the tiopronin–AuNPs are distributed in the cytoplasm of EMT-6 cells (a movie is provided as Supplementary Material—file: Fig_8B.mpg). The results confirmed that the nanoparticles are internalized into cytoplasm. Furthermore, a simple manual counting of the nanoparticles revealed that their average aggregate size is ~400 nm (Fig. 9), and that their localization in cells is rather uniform with respect to the nucleus and cell membrane. The resolution of TXM is not sufficient to resolve single nanoparticles as in TEM: only aggregates in the endosomes are imaged, but the possibility of tomographic reconstruction complements the TEM. With the full 3D capability of TXM, we can corroborate the TEM observations and definitely conclude that there are no nanoparticles in the nucleus. These results indicate that just the small size alone is not a sufficient factor to allow the localization of nanoparticles in the cell nucleus and additional surface modifications are required to achieve it [49].

Conclusion

We demonstrated the synthesis of Au nanoparticles modified with tiopronin by synchrotron X-ray irradiation. These particles are stable in cell medium with 10% fetal bovine serum and are quite biocompatible. A combination of three complementary methods (TEM, ICP-MS, and TXM) was used to quantitatively and microscopically investigate the cellular uptake of such nanoparticles. The nanoparticles were found near the cell nucleus periphery, but not inside the cell nucleus.

Acknowledgments This research was supported by the National Science and Technology Program for Nanoscience and Nanotechnology, the Thematic Research Project of Academia Sinica, the Biomedical Nano-Imaging Core Facility at National Synchrotron Radiation Research Center (Taiwan), the Fonds National Suisse pour la Recherche Scientifique, and by the Center for Biomedical Imaging (CIBM, supported by the Louis-Jeantet and Leenards foundations). The Advanced Photon Source was supported by the US Department of Energy, Office of Science, Office of Basic Energy Sciences, under the Contract No. DE-AC02-06CH11357.

References

1. Daniel MC, Astruc D (2003) Chem Rev 104:293–346
2. Dahl JA, Maddux BLS, Hutchison JE (2007) Chem Rev 107:2228–2269
3. Funston AM, Mulvaney P, Murray RW (2009) Langmuir 25:13840–13851
4. Brust M, Fink J, Bethell D, Schiffrin DJ, Kiely CJ (1995) Chem Commun 16:1655–1656

5. Brust M, Schiffrin DJ, Bethell D, Kiely CJ (1995) Adv Mater 7:795–797
6. Brown LO, Hutchison JE (1997) J Am Chem Soc 119:12384–12385
7. Chen S, Murray RW (1998) Langmuir 15:682–689
8. Templeton AC, Chen S, Gross SM, Murray RW (1998) Langmuir 15:66–76
9. Schaaff TG, Whetten RL (2000) J Phys Chem B 104:2630–2641
10. Pasquato L, Pengo P, Scrimin P (2004) J Mater Chem 14:3481–3487
11. Price RC, Whetten RL (2005) J Am Chem Soc 127:13750–13751
12. Bertino MF, Sun ZM, Zhang R, Wang LS (2006) J Phys Chem B 110:21416–21418
13. Jin R (2008) Agew Chem Int Ed 47:6750–6753
14. Wu Z, Suhan J, Jin R (2009) J Mater Chem 19:622–626
15. Zhu Y, Qian H, Zhu M, Jin R (2010) Adv Mater 22:1915–1920
16. Tang Z, Xu B, Wu B, Germann MW (2010) J Am Chem Soc 132:3367–3374
17. Heaven MW, Dass A, White PS, Holt KM, Murray RW (2008) J Am Chem Soc 130:3754–3755
18. Jadzinsky PD, Calero G, Ackerson CJ, Bushnell DA, Kornberg RD (2007) Science 318:430–433
19. Seino S, Kinoshita T, Nakagawa T, Kojima T, Taniguci R, Okuda S, Yamamoto T (2008) J Nanopart Res 10:1071–1076
20. Ma Q, Moldovan N, Mancini DC, Rosenberg RA (2000) Appl Phys Lett 76:2014–2016
21. Karadas F, Ertas G, Ozkaraoglu E, Suzer S (2004) Langmuir 21:437–442
22. Cai XQ, Wang CL, Chen HH, Chie CC, Lai SF, Chen YY, Hua TE, Kempson IM, Hwu Y, Yang CS, Margaritondo G (2010) Nanotechnology 21:335604
23. Wang CH, Liu CR, Wang CL, Hua TE, Lee KH, Hwu YK (2008) J Phys D Appl Phys 41:195301–195308
24. Wang CH, Hua TE, Chien CC, Yu YL, Yang TY, Liu CJ, Leng WH, Hwu YK, Yang YC, Kim CC, Je JH, Chen CH, Lin HM, Margaritondo G (2007) Mater Chem Phys 106:323–329
25. Wang CL, Hso BJ, Lai SF, Chen WC, Chen HH, Chen YY, Chien CC, Cai XQ, Kempson IM, Hwu Y, Margaritondo G (2011) Nanotechnology 22:065605
26. Alkilany AM, Nagaria PK, Hexel CR, Shaw TJ, Murphy CJ, Wyatt MD (2009) Small 5:701–708
27. Chithrani BD, Ghazani AA, Chan WCW (2006) Nano Lett 6:662–668
28. Chithrani BD, Chan WCW (2007) Nano Lett 7:1542–1550
29. Nativo P, Prior IA, Brust M (2008) ACS Nano 2:1639–1644
30. Chu YS, Yi JM, De Carlo F, Shen Q, Lee WK, Wu HJ, Wang CL, Wang JY, Liu CJ, Wang CH, Wu SR, Chien CC, Hwu YK, Tkachuk A, Yun W, Feser M, Liang KS, Je JH, Margaritondo G (2008) Appl Phys Lett 92:103119–103123
31. Chen YT, Chen TY, Yi J, Chu YS, Lee WK, Wang CL, Kempson IM, Hwu Y, Gajdosik V, Margaritondo G (2011) Opt Lett 36:1269–1271
32. Syme CD, Sirimuthu NM, Faley SL, Cooper JM (2010) Chem Commun 46:7921–7923
33. Sirimuthu NMS, Syme CD, Cooper JM (2010) Anal Chem 82:7369–7373
34. Le Gros MA, McDermott G, Larabell CA (2005) Curr Opin Struck Biol 15:593–600
35. Larabell CA, Le Gros MA (2004) Mol Biol Cell 15:957–962
36. Hsu PC, Wang CH, Yang TY, Hwu YK, Lin CS, Chen CH, Chang LW, Seol SK, Je JH, Margaritondo G (2007) J Vac Sci Technol A 25:615–620
37. Kim YG, Oh SK, Crooks RM (2003) Chem Mater 16:167–172
38. Liu CJ, Wang CH, Chen ST, Chen HH, Leng WH, Chien CC, Wang CL, Kempson IM, Hwu Y, Lai TC, Hsiao M, Yang CS, Chen YJ, Margaritondo G (2010) Phys Med Biol 55:930–945
39. Aft RL, Lewis JS, Zhang F, Kim J, Welch MJ (2003) Cancer Res 63:5496–5504
40. Huang FK, Chen WC, Lai SF, Liu CJ, Wang CL, Wang CH, Chen HH, Hua TE, Chen YY, Wu MK, Hwu Y, Yang CS, Margaritondo G (2010) Phys Med Biol 55:469–482
41. Chen HH, Chien CC, Petibois C, Wang CL, Chu YS, Lai SF, Hua TE, Chen YY, Cai XQ, Hwu Y, Margaritondo G (2011) J Nanobiotechnology 9(1):14
42. Wang CH, Liu CJ, Chien CC, Chen HT, Hua TE, Leng WH, Chen HH, Kempson IM, Hwu Y, Hsiao M, Lai TC, Wang JL, Yang CS, Lin HM, Chen YJ, Margaritondo G (2011) Mater Chem Phys 126:352–356
43. Wörle-Knirsch JM, Pulskamp K, Krug HF (2006) Nano Lett 6:1261–1268
44. Yen HJ, Hsu SH, Tsai CL (2009) Small 5:1553–1561
45. Castaneda L, Valle J, Yang N, Pluskat S, Slowinska K (2008) Biomacromolecules 9:3383–3388
46. De La Fuente JM, Berry CC, Riehle MO, Curtis AS (2006) Langmuir 22:3286–3293
47. Mobius W, van Donselaar E, Ohno-Iwashita Y, Shimada Y, Heijnen HF, Slot JW, Geuze HJ (2003) Traffic 4:222–231
48. Pelkmans L, Burli T, Zerial M, Helenius A (2004) Cell 118:767–780
49. Tkachenko AG, Xie H, Liu Y, Coleman D, Ryan J, Glomm WR, Shipton MK, Franzen S, Feldheim DL (2004) Bioconjug Chem 15:482–490